Science in China Series D: Earth Sciences

Springer

www.scichina.com
earth.scichina.com
www.springerlink.com

Zircon U-Pb SHRIMP ages of the Taiping (calc-alkaline)-Huangshan (alkaline) composite intrusion: Constraints on Mesozoic lithospheric thinning of the southeastern Yangtze Craton, China

XUE HuaiMin[1†], WANG YingGeng[2], MA Fang[3], WANG Cheng[4], WAN DeEn[2] & ZUO YanLong[2]

[1] Institute of Geology, Chinese Academy of Geological Sciences, Beijing 100037, China;
[2] 332 Team, Bureau of Geology and Mineral Resources of Anhui Province, Tunxi 245000, China;
[3] School of Earth and Space Sciences, Peking University, Beijing 100871, China;
[4] Department of Programming and Ground, World Geological Park of Huangshan, Huangshan 245000, China

The Taiping-Huangshan composite intrusion is a unique complex with characteristics changing from calc-alkaline (Taiping intrusion) to alkaline (Huangshan intrusion). Huangshan intrusion samples show a spectacular tetrad effect in their REE distribution patterns as well as non-CHARAC (charge-and-radius-controlled) trace element behavior, indicating a highly evolved late-stage magma component. This composite intrusion provides a rare opportunity to investigate the variance of tectonic setting and lithospheric thinning of the southeastern Yangtze Craton in late Mesozoic era. Zircon SHRIMP U-Pb analyses yield an emplacement age of 140.6±1.2 Ma for the Taiping intrusion, and ages of 127.7±1.3, 125.7±1.4, 125.1±1.5, and 125.2±5.5 Ma for four samples from the Huangshan intrusion respectively. The ages for four different phases of the Huangshan intrusion agree within their small analytical errors, indicating that the emplacement was in a short time. The Taiping and Huangshan intrusions are intimately associated, but there is about 15 Ma interval between their intrusion, and the magma characters change from calc-alkaline to alkaline without transition. This probably corresponds to lithospheric thinning of the southeastern Yangtze Craton. This event possibly happened from about 141 Ma (the emplacement age of the Taiping intrusion), to 128 Ma (start of emplacement of the Huangshan intrusion). The thinning mechanism is dominantly delamination.

SHRIMP U-Pb dating, lithospheric thinning, Huangshan intrusion, Taiping intrusion, Yangtze Craton, Mesozoic

In the last twenty years, one of the important developments in lithosphere research of eastern China is the discovery of large scale thinning of the continental lithosphere during the Mesozoic and Cenozoic eras[1−16]. The idea was first raised from east part of the North China Craton. This research work is still mainly focused on the North China Craton, with seldom reference to other areas of eastern China, although some geologists hold that the lithosphere of southeastern China had also undergone huge thinning[7,17,18]. Although there are still many debates about the genesis of A-type granite, it has been generally accepted that they are emplaced at an extensional or non-compressional tectonic setting[19−23], with their petrogenesis mostly attributed to upwelling of hot asthenospheric mantle. Generally, thinning of extended crust is closely associated with thermal activity (e.g., upwelling of asthenospheric mantle or infusing of basic magma). Upwelling of asthenospheric mantle not

Received February 19, 2009; accepted May 22, 2009
doi: 10.1007/s11430-009-0133-9
†Corresponding author (email: huaiminx@sina.com)
Supported by National Natural Science Foundation of China (Grant Nos. 40772048, 40503006 and 40472035) and China Geological Survey (Grant No. 1212010711814)

Citation: Xue H M, Wang Y G, Ma F, et al. Zircon U-Pb SHRIMP ages of the Taiping (calc-alkaline)-Huangshan (alkaline) composite intrusive: Constraints on Mesozoic lithospheric thinning of the southeastern Yangtze Craton, China. Sci China Ser D-Earth Sci, 2009, 52(11): 1756-1770, doi: 10.1007/s11430-009-0133-9

only provided heat and material necessary for the genesis of A-type granitic magma, but it also facilitated wide regional partial melting of continental crust. Therefore, A-type granites in a continental setting may indicate the time, process, and dynamic mechanism of lithospheric thinning and asthenospheric upwelling.

The Taiping-Huangshan composite intrusion in southern Anhui Province is one of the representatives of Cretaceous large scale platonism in the lower Yangtze River region of China. Our research on the geochemistry of the composite intrusion discovered that the Huangshan intrusion has typical characteristics of A-type granite, and its REE chemistry exhibits a pronounced "tetrad effect", which represents a highly evolved late-stage magma composition[24]. But the Taiping intrusion is a typical I-type granite. Geochemical characteristics thus change from calc-alkaline (the Taiping intrusion) to alkaline (the Huangshan intrusion), which gives a rare chance to study late-Mesozoic tectonic environments, and the timing and mechanism of lithospheric thinning of the southeastern Yangtze Craton. Until now, there has been little work on the composite intrusion.

There are some isotopic datings mainly obtained in 1980's of mostly poor quality; some are even erronous, which led some researchers ascribed the Taiping intrusion to the Indo-Chinese event (about 230 Ma)[25−27]. This paper reports some newly gained precise zircon SHRIMP ages, which constrains the timing of magmatism and the initiation of the lithospheric thinning, based on the time of change from calc-alkaline to alkaline geochemical affinity.

1 Geological background

1.1 Regional interpretations

The Taiping-Huangshan composite intrusion is located in the Jiangnan uplift belt of the southeastern Yangtze Craton. Tectonic style of the uplift belt remains in dispute. It was initially called the "Jiangnan old continent" or "Jiangnan-Xuefeng old continent"[28]. Guo et al.[29] considered it as a fold belt comprising Neoproterozoic island arc rocks. Zhu[30] considered that this uplift belt is a nappe formed by Indo-Chinese event delamination within continental lithosphere. Xu et al.[31] considered that the so-called Jiangnan uplift belt is an Alpine-style nappe from the Huaxia block (South China). Qiu et al.[32] proposed that the Jiangnan uplift belt exposed in the Xuefeng Mountain area was a complex intracontinental orogenic unit developed since the Caledonian. Zhu and Liu[33] considered that the Jiangnan uplift belt exposed in southern Anhui Province is a intracontinental orogenic unit of Indo-Chinese to early Yanshan timing (from about 230 to 170 Ma), formed under continent-continent collision between the North China plate plus the Yangtze Plate in the north, and South China Plate in the south.

1.2 Geology and samples of the intrusion

The Taiping-Huangshan composite intrusion is elongated N-S and about 350 km^2 in area. The outcrop area of the Taiping intrusion in the northwest is about twice that of the Huangshan intrusion, and shows relatively low relief. The Huangshan intrusion has rugged mountainous relief, and forms the southeastern part of the composite intrusion. Clear intrusive relationship occurs between the two components showing that the Taiping intrusion is older than the Huangshan intrusion. The country rocks are Late-proterozoic to Precambrian metamorphosed sedimentary-volcanic rocks and carbonates, including sandstone, siltstone, mudstone, slate, carbonaceous limestone, tuff, and rhyolite.

Internally, the Taiping and Huangshan intrusions are composite plutons with several pulses of magma. The Taiping intrusion can be divided approximately into three stages, based on relation of lithofacies in field; the rocks are medium-grained porphyritic monzogranite, fine-grained monzogranite and medium-grained granodiorite respectively. The main part of the Huangshan intrusion is porphyritic alkali feldspar granite, which forms >90% of the outcrop, including coarse-grained porphyritic alkali-feldspar granite and medium- to fine-grained porphyritic alkali-feldspar granite, with a gradual transitional relationship in the field. There is minor medium-grained monzogranite, outcropping at the south margin of the intrusion, with some also outcropping at the northwest part of the intrusion in the vicinity of contact with the Taiping intrusion.

The samples prepared for age analysis were collected from medium-grained granodiorite of the Taiping intrusion (sample TP-1) and different stages or phases of the Huangshan intrusion (samples HS-1, HS-2, HS-3 and HS-4). Locations of sampling are shown in Figure 1(b), and their geochemical and Sr-Nd isotopic compositions are presented in Table 1.

Granodiorite sample TP-1 has a medium-grained equigranular to granitic texture. The rock is composed

mainly of plagioclase (~45%), K-feldspar (~25%), quartz (~15%), and biotite (~15%); with zoning in some plagioclase crystals.

Coarse-grained porphyritic alkali-feldspar granite sample HS-2 has phenocrysts of large perthitic K-feldspar (~25%) up to 1 cm long. They bear many small inclusions of plagioclase (albite) and biotite. The matrix has a coarse-grained granulitic texture, and is composed of albite (~30%), perthite (~30%), quartz (~30%) and biotite (~10%).

Samples HS-1 and HS-3 are porphyritic alkali-feldspar granites. The groundmass of HS-1 is finer-grained than in HS-3. The phenocrysts of both samples are perthite and comprise about 15% of both samples; the size are usually 0.3 cm×0.5 cm, the maximum is 0.5 cm×1.0 cm. The matrix comprises of perthite (~40%), albite (~30%), quartz (~20%), with minor biotite (~5% or so). Sample HS-4 is medium-grained monzogranite, with a homogeneous granulitic texture. It comprises plagioclase (albite-oligoclase), K-feldspar and quartz (~30% respectively) and biotite (~10%).

1.3 Geochemical characters

The Taiping intrusion shows large variations in chemical compositions (with SiO_2=65.47%—76.96%); and in terms of CIPW norms they are mostly monzogranite, but some samples grade to syenogranite on the QAP diagram (Figure 2(a)). The Huangshan intrusion displays a limited range in chemical composition, and is characterized by high SiO_2 contents (SiO_2>75%), low CaO (0.51%—0.86%), poor in MgO and is rich in alkalis (Na_2O+K_2O=6.95%—7.37%), and high FeO*/MgO ratios (8.28—87.20). Thus it is a typical A-type granite.

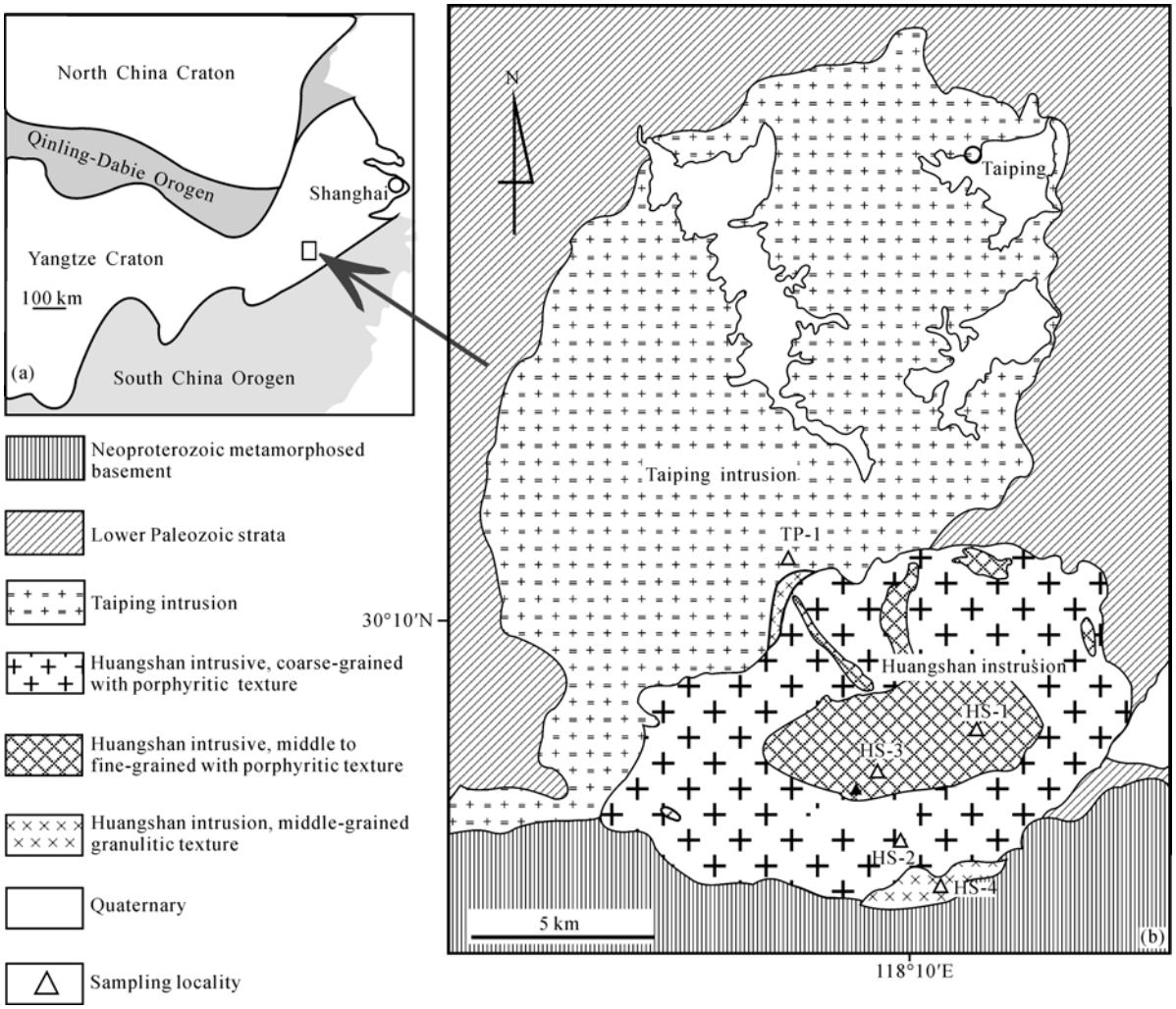

Figure 1 Schematic geological map of the Taiping-Huangshan composite intrusion (modified from 1∶50000 scale geological maps of Taiping County and Tangkou).

Table 1 Major (wt%) and trace element (ppm) abundances and Sm-Nd and Rb-Sr isotopic data of representative samples from the Taiping-Huangshan composite intrusion[a)]

	Huangshan intrusive				Taiping intrusive
	HS-1	HS-2	HS-3	HS-4	TP-1
SiO_2	75.25	76.75	75.41	76.3	68.95
TiO_2	0.19	0.11	0.07	0.03	0.48
Al_2O_3	12.81	11.61	13.32	13.12	14.74
Fe_2O_3	0.48	0.65	0.64	0.08	0.93
FeO	1.07	0.74	0.47	0.8	1.85
MnO	0.04	0.04	0.04	0.03	0.06
MgO	0.17	0.16	0.06	0.01	1.14
CaO	0.75	0.86	0.51	0.54	2.94
Na_2O	3.36	3.44	3.97	4.38	3.46
K_2O	5.3	3.96	4.59	4.28	3.78
P_2O_5	0.03	0.01	0.01	<0.01	0.15
H_2O	0.62	0.6	0.6	0.5	0.76
CO_2	0.18	0.71	0.27	0.14	0.3
Total	100.25	99.64	99.96	100.21	99.54
Rb	434	510	696	759	181
Sr	45.9	20.9	13.5	14.2	358
Ba	166	41.2	33	14.9	367
Zr	208	181	113	125	148
Hf	7.56	8.59	6.25	9.18	4.62
Sc	2.57	2.42	2.25	1.22	5.81
Nb	34.9	77	49.8	68	15.4
Ta	5.99	8.71	13.1	14.2	1.62
Ga	22.3	23.2	26.4	29.7	18.4
Th	56.1	71.8	41.1	55.9	19.00
U	8.46	18.3	12.8	15.2	4.44
Y	71.3	147	126	218	14.6
La	77.5	45.6	25.3	23.5	29.00
Ce	157	107	55.9	64.2	55.5
Pr	18.5	13.8	8.35	9.42	6.47
Nd	64.6	53.4	33.4	40.8	24.3
Sm	12.8	14.8	11.2	15.9	4.45
Eu	0.54	0.22	0.14	0.04	0.99
Gd	11.2	14.4	10.3	16.1	3.85
Tb	1.83	3.05	2.41	3.68	0.51
Dy	10.8	20.9	16.7	25.2	2.61
Ho	2.18	4.47	3.6	5.4	0.48
Er	7.04	14.6	12.6	17.5	1.51
Tm	1.08	2.28	2.2	2.74	0.2
Yb	7.62	15.6	16.3	18.7	1.43
Lu	1.12	2.28	2.44	2.77	0.23
ΣREE	373.81	312.40	200.84	245.95	131.53
$(La/Yb)_N$	6.87	1.98	1.05	0.85	11.70
Eu/Eu*	0.13	0.05	0.04	0.01	0.71
$(Nb/La)_N$	0.44	1.66	1.94	2.95	0.52
Rb/Sr	9.46	24.40	51.56	53.45	0.51
Zr/Hf	27.51	21.07	18.08	13.62	32.03
K/Rb	101.33	64.43	54.72	46.79	173.29
$TE_{1,3}$	1.03	1.10	1.09	1.08	0.96
$^{87}Rb/^{86}Sr$	30.80	86.02	206.7	200.7	1.460
$^{87}Sr/^{86}Sr\pm2\sigma$	0.765539±15	0.872459±15	1.085563±14	1.094434±15	0.713491±15
$(^{87}Sr/^{86}Sr)_i$	0.707				0.710462
$^{147}Sm/^{144}Nd$	0.1237	0.1740	0.2055	0.2455	0.1154
$^{143}Nd/^{144}Nd\pm2\sigma$	0.512338±13	0.512391±13	0.512411±13	0.512436±12	0.512245±13
$\varepsilon_{Nd}(t)$	–4.66	–4.45	–4.57	–4.74	–6.21
T_{DM2}/Ga	1.30	1.28	1.24	1.33	1.44

a) Degree of the tetrad effect $TE_{1,3}=(T_1\times T_3)^{0.5}$, $T_1=(Ce^*\times Pr^*)^{0.5}$, $T_3=(Tb^*\times Dy^*)^{0.5}$, $Ce^*=Ce_{cn}/(La_{cn}^{2/3}\times Nd_{cn}^{1/3})$, $Pr^*=Pr_{cn}/(La_{cn}^{1/3}\times Nd_{cn}^{2/3})$, $Tb^*=Tb_{cn}/(Gd_{cn}^{2/3}\times Ho_{cn}^{1/3})$, $Dy^*=Dy_{cn}/(Gd_{cn}^{1/3}\times Ho_{cn}^{2/3})$, Ln_{cn}=chondrite-normalized lanthanide concentration. The initial isotopic data are recalculated for 128 Ma and 141 Ma for the Huangshan and Taiping intrusion respectively. Chondritic uniform reservoir: $^{147}Sm/^{144}Nd=0.1967$, $^{143}Nd/^{144}Nd=0.512638$. Model age of two stage $T_{DM2}=T_{DM1}-(T_{DM1}-t)(f_{cc}-f_s)/(f_{cc}-f_{DM})$, $f_{cc}=-0.4$, $f_{DM}=0.08592$, t=emplacement ages of granitic intrusion. Depleted mantle: $^{147}Sm/^{144}Nd=0.2137$, $^{143}Nd/^{144}Nd=0.513151$.

Aluminum saturation indices of the Taiping intrusion are mainly metaluminious; with a few being peraluminous (Figure 2(b)). In contrast the Huangshan intrusion grades from metaluminious to peraluminous, and locally strongly peraluminous. The Taiping intrusion corresponds to the "I-type granite" field on the discrimination diagram (Figure 2(c)) and "syncollisional and/or volcanic-arc granite" field on the Y-Nb tectonic discrimination diagram of Pearce et al.[34] (Figure 2(d)). On the other hand, all samples of the Huangshan intrusion fall in the field of A-type granite (Figure 2(c)) and the "within-plate granite" field (Figure 2(d)). They have the characteristics of A_2-type granite formed in a post-orogenic setting[24].

The Huangshan intrusion exhibits a strong "tetrad effect" of REE distribution patterns (Figure 2(e)), which is infrequent partition model of REE, only seen in highly evolved magmatic differentiates with strong hydrothermal interactions[35−38] or in non-hydrothermal settings in the deep crust[39], and can be interpreted as transitional between the end-members of magmatic and high-temperature hydrothermal systems[35,38] or in the setting has undergone strong fractionation of plagioclase[39]. Corresponding to the "tetrad effect" of REE distribution patterns, behaviors of many trace elements of the Huangshan granite also show obvious aberrance, termed by Bau[35] as non-CHARAC behavior: K/Rb ratios are usually low (except one or two samples at about 100, but most are less than 65, while K/Rb ratios of ordinary granitoid are usually greater than 150), high K/Ba ratios (among 265−2384, while K/Ba ratios of ordinary continental rocks are less than 50), low Zr/Hf ratios (only 27.5−13.6, while Zr/Hf ratios of most continental rocks are 38 ± 2). Besides these, the Huangshan intrusion exhibits strong negative Eu anomalies (δEu=0.01−0.13) and strong depleted Ba, Sr (Figure 2(f)). In sharp contrast, the Taiping intrusion shows stronger enrichment of the LREE over the HREE, has only slight negative Ba and Sr anomalies (Figure 2(h)), weak negative Eu anomalies; and therefore has no "tetrad effect" (Figure 2(g)).

The initial $^{87}Sr/^{86}Sr$ ratio of the Huangshan granite is about 0.707, lower than that of Taiping intrusion, which is about 0.710. The $\varepsilon_{Nd}(t)$ values are –4.45 to –4.87, higher than that of the Taiping intrusion, which are –6.21 to –6.40. The Nd two-stage model age (T_{DM2}) of the Huangshan intrusion is 1.24 to 1.33 Ga (average 1.29 Ga), lower than that for the Taiping intrusion (1.44−1.45 Ga).

2 Zircon morphology and analysis methods

2.1 Zircon morphology

The zircon crystals from the Taiping intrusion are euhedral prisms with aspect ratios of 1/2 to 1/3. Most zircon grains exhibit clear oscillatory zoning, indicating a magmatic origin. Some zircons contain relicts of inherited zircon in their inner parts.

The zircons from the Huangshan granite have very high U contents. Except the sample HS-1, the outermost of the zircon crystals from the other samples have developed characteristic black rims in CL images (very high U content). Many zircon grains suffered strong damage due to radioactivity, and exhibiting abundant fissures in the inner parts of the grains. Some zircons are entirely metamict. As shown in Figure 3, zircons from the Huangshan granite are euhedral prisms with aspect ratios usually 1/4−1/2. Prismatic faces are much more developed than pyramidal terminations. These zircon grains exhibit clear oscillatory zoning, indicating a magmatic in origin. Many zircon grains include small inclusions of biotite and potassium feldspar, indicating that zircons crystallized at the same time or slightly later than the crystallization of essential minerals. Most zircon grains have a black rim in CL images corresponding with inner oscillatory zoning, and some black rims are enlarged (e.g., sample HS-3), and in some cases cuts oscillatory zoning (e.g., sample HS-3). This shows that the black rim formed later than the main time of zircon grains, and also indicates clear U enrichment in the late stage of magma evolvement. We consider that the black rims of zircons were formed by interaction of highly evolved magmatic differentiates with high-temperature hydrothermal fluids, consistent with the whole rock "tetrad effect" REE distribution patterns and the non-CHARAC behavior of some trace elements.

2.2 Analysis methods

Major and trace element abundances were determined at the National Research Center for Geoanalysis, Chinese Academy of Geological Sciences, and major and most trace elements were determined by the X-ray fluorescence (XRF) method using a Japanese 3080 spectrome ter and Rigaku-2100 respectively. Analytical errors

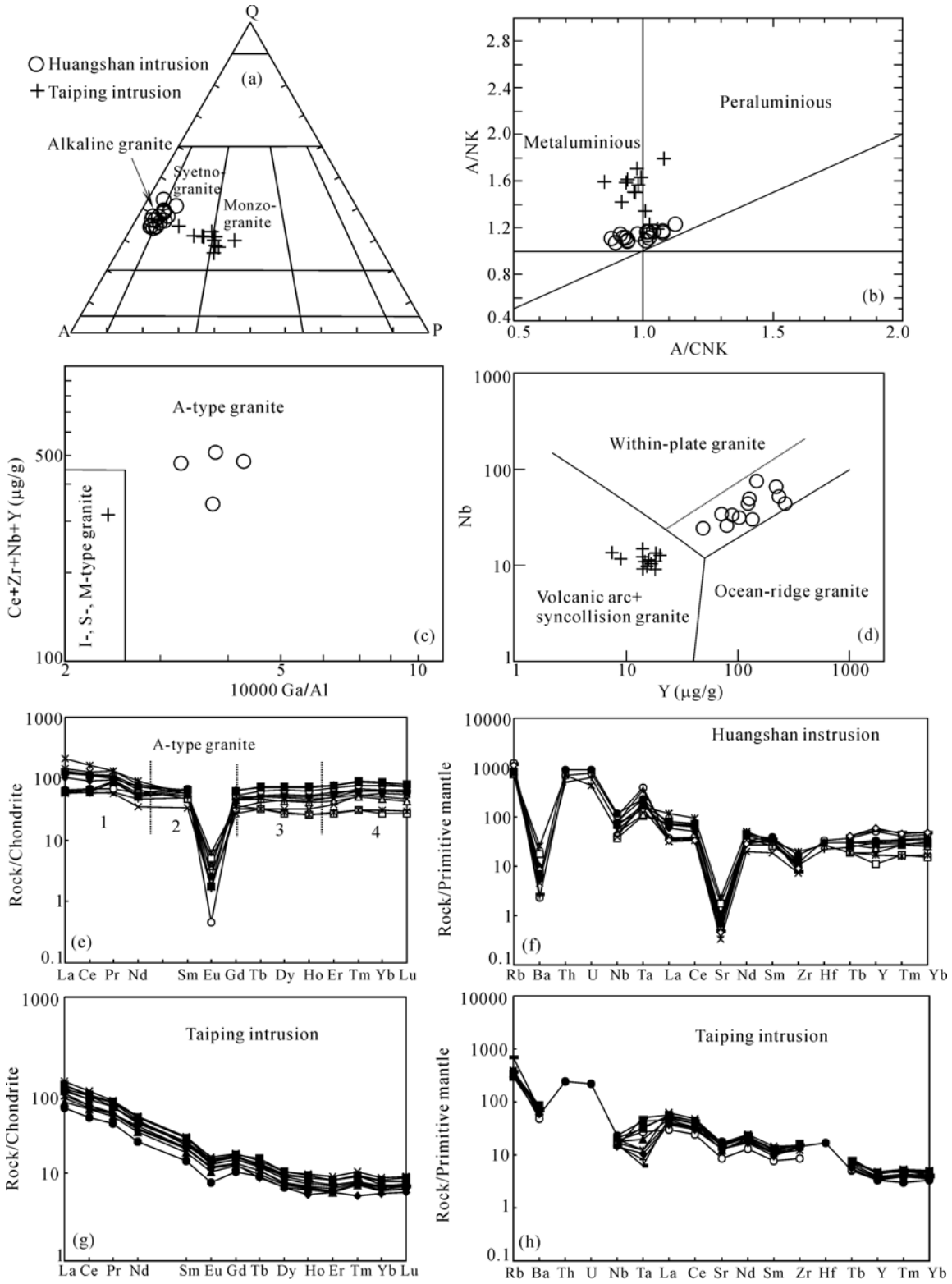

Figure 2 Geochemical diagrams of the Taiping-Huangshan composite intrusive. (a) Q-A-P normative compositions[40]; (b) A/NK vs. A/CNK diagram; (c) Ce+Zr+Nb+Y vs. 10000 Ga/Al classification diagram[19]; (d) Nb vs. Y tectonic discrimination[34]; (e), (g) chondrite-normalized REE-patterns (chondrite data from Boynton[41]); (f), (h) primitive mantle normalized incompatible element patterns (primitive upper mantle from McDonough and Sun[42]). Data sources: Xue et al.[24]; Chen et al.[43]; the geology reports of Taiping County and Tangkou, published at a scale of 1∶50000.

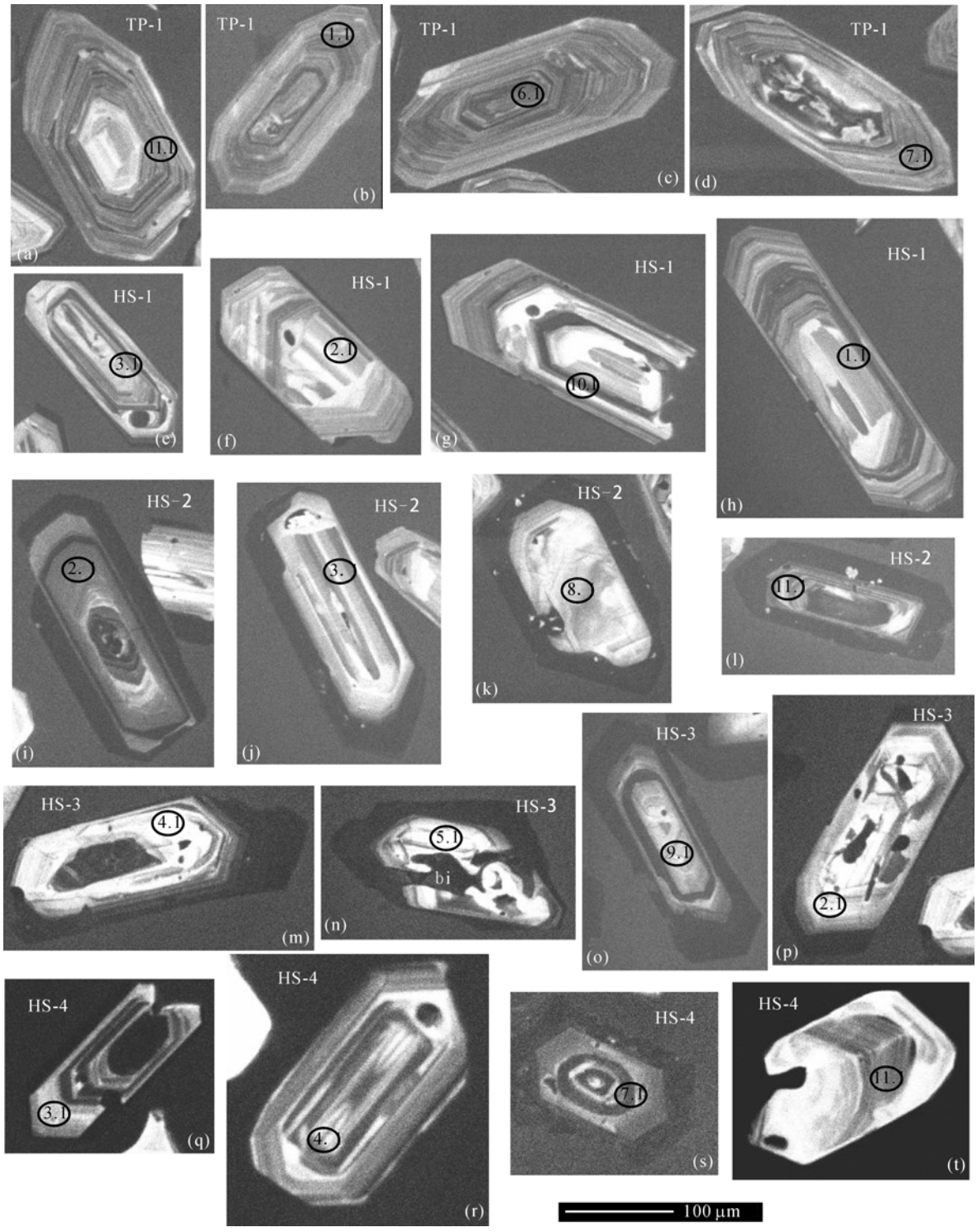

Figure 3 CL images of dated zircon crystals from the Taiping-Huangshan composite intrusive. Bi, Bi inclusions.

(RSD) are <0.5% for major elements, ~5% for Ba, <3% for other trace elements. Rare earth elements and V, Cr, Ni, Co, Cu, Pb, U, Th, Ta and Hf were measured using ICP-MS (TJA-PQ-ExCell), the uncertainties vary from <5% to <10% depending on the concentration levels. All Sm-Nd and Rb-Sr isotopic data were obtained at the isotope laboratory, Institute of Geology and Geophysics, Chinese Academy of Sciences using standard techniques, which are broadly the same as described by Jahn et al.[44].

Zircons for isotopic analysis were processed using conventional mineral separation techniques from about 10 kg rock samples, and finally hand-picked under a binocular microscope according to shape, homogeneity, transparency and color. The zircon grains, together with standard zircon crystals of SL13 and several TEM grains, were mounted and polished to expose their mid sections. The mounts were then rigourously cleaned and gold coated. U-Pb zircon analyses for sample HS-4 was performed using the sensitive, high-resolution ion microprobe (SHRIMP II) at the Beijing SHRIMP Center, Institute of Geology, Chinese Academy of Geological Sciences (CAGS). The other four samples were undertaken on a SHRIMP-II instrument at Curtin University of Technology, Western Australia. The instrument was controlled and data acquired from a remote control center in the Beijing SHRIMP center, Institute of Geology, CAGS, Beijing. The SHRIMP spots were selected according to CL images, combined with reflected and transmitted light photographs, in order to avoid mineral inclusions and internal imperfections such as cracks. Instrumental conditions and data acquisition were broadly the same as described by Williams[45]. During routine zircon analysis, the data were collected over five cycles through the mass stations. The beam was focused to a spot of about 25－30 μm in diameter and the analyses with a 4.5 nA secondary beam at a mass resolution of about 5000. A zircon of known composition (SL13, 572 Ma, 238 ppm U) was used to determine the U, Th, and Pb content of unknown zircons, and the zircon TEM standard (with a $^{206}Pb/^{238}U$ age of 417 Ma) was used to correct instrumental U-Pb elemental fractionation. The formula used for Pb-U calibration is $Pb/U=A(UO/U)^{2}$[46]. The ^{204}Pb method was employed for the common lead correction. Uncertainties are reported at the 1σ level (isotope ratios; cf. Table 2) and at the 95% confidence level in the text. The data were reduced and assessed using the SQUID and Isoplot programs of Ludwig[47].

3 Results

The SHRIMP zircon U-Pb analytical results are listed in Table 2. The zircons all have high Th/U ratios, mostly larger than 0.5; which combined with their morphology and internal structure, it can be ascertained that they are all magmatic in origin.

Table 2 shows that the apparent ages of the zircons (common Pb is corrected by ^{204}Pb) from the Taiping intrusion are concentrated between 138－146 Ma. In the $^{206}Pb/^{238}U$-$^{207}Pb/^{235}U$ concordia diagram, all samples are located on or close to concordia (Figure 4), with weighted mean $^{206}Pb/^{238}U$ age of 140.6 ± 1.2 Ma (MSWD=0.97). Excluded is analysis point 5.1, in which $^{206}Pb/^{238}U$ apparent age is as high as 240 ± 4 Ma and is probably inherited zircon.

For the Huangshan intrusion, $^{206}Pb/^{238}U$ apparent ages of zircons from sample HS-1 are 124－146 Ma, with a weighted mean age of 127.7 ± 1.3 Ma (MSWD= 0.84); the $^{206}Pb/^{238}U$ apparent ages of zircons from sam-

Table 2 Zircon U-Pb SHRIMP dating results of Taiping-Huangshan composite intrusive[a)]

Point	Content (μg/g)			Th/U	f^{206}(%)	Ratio (±%)			Age (Ma)	
	Pb*	U	Th			$^{206}Pb*/^{238}U$	$^{207}Pb*/^{235}U$	$^{207}Pb*/^{206}Pb*$	$^{206}Pb*/^{238}U$	$^{208}Pb*/^{232}Th$
Taiping intrusion										
TP-1-1.1	19.8	1051	704	0.67	0.43	0.02186 (1.5)	0.1460 (4.1)	0.0484 (3.8)	139.4±2.1	136.4±3.7
TP-1-2.1	16.5	854	460	0.54	0.74	0.02233 (1.5)	0.1447 (4.8)	0.0470 (4.6)	142.4±2.1	137.9±5.0
TP-1-3.1	9.99	521	188	0.36	0.79	0.02214 (1.5)	0.139 (7.6)	0.0455 (7.4)	141.1±2.2	135±10
TP-1-4.1	4.98	256	171	0.67	1.06	0.02243 (1.7)	0.201 (9.8)	0.0650 (9.6)	143.0±2.4	158±12
TP-1-5.1	10.9	333	65	0.20	0.55	0.03788 (1.6)	0.389 (4.8)	0.0746 (4.6)	239.7±3.7	196±32
TP-1-6.1	21.1	1103	990	0.90	0.41	0.02220 (1.5)	0.1512 (3.3)	0.0494 (2.9)	141.5±2.0	134.9±2.8
TP-1-7.1	15.8	843	458	0.54	0.77	0.02171 (1.5)	0.1378 (4.7)	0.0461 (4.5)	138.4±2.0	129.3±4.6
TP-1-8.1	15.6	834	382	0.46	0.12	0.02175 (1.6)	0.1540 (2.9)	0.0514 (2.5)	138.7±2.1	142.6±3.7
TP-1-9.1	16.2	861	557	0.65	0.54	0.02184 (1.5)	0.1361 (4.7)	0.0452 (4.4)	139.3±2.0	141.7±4.3
TP-1-10.1	13.5	715	296	0.41	0.49	0.02190 (1.5)	0.1515 (4.6)	0.0502 (4.3)	139.6±2.1	142.1±6.0
TP-1-11.1	13.4	677	265	0.39	0.60	0.02283 (1.5)	0.1498 (4.8)	0.0476 (4.5)	145.5±2.1	140.7±6.5
TP-1-12.1	19.3	1027	572	0.56	0.20	0.02188 (1.5)	0.1470 (5.6)	0.0487 (5.4)	139.5±2.0	136.4±5.7

(*To be continued on the next page*)

(*Continued*)

Point	Content (μg/g)			Th/U	f^{206}(%)	Ratio (±%)			Age (Ma)	
	Pb*	U	Th			$^{206}Pb^*/^{238}U$	$^{207}Pb^*/^{235}U$	$^{207}Pb^*/^{206}Pb^*$	$^{206}Pb^*/^{238}U$	$^{208}Pb^*/^{232}Th$
TP-1-13.1	10.4	553	201	0.36	0.24	0.02188 (1.5)	0.1525 (4.6)	0.0505 (4.4)	139.6±2.1	143.0±6.7
Huangshan intrusion										
HS-1-1.1	4.97	292	213	0.73	0.00	0.01995 (1.6)	0.1524 (3.8)	0.0554 (3.4)	127.4±2.0	132.8±3.9
HS-1-2.1	4.19	237	119	0.50	1.81	0.02024 (1.7)	0.1187 (8.3)	0.0425 (8.2)	129.2±2.1	109.9±7.1
HS-1-3.1	2.84	161	105	0.65	0.00	0.02065 (1.7)	0.1769 (4.6)	0.0621 (4.3)	131.7±2.3	149.6±5.5
HS-1-4.1	2.71	156	97	0.62	3.97	0.01940 (2.2)	0.089 (35)	0.033 (35)	123.9±2.7	97±18
HS-1-5.1	4.49	255	143	0.56	2.16	0.02004 (1.8)	0.113 (16)	0.0407 (16)	127.9±2.3	113±12
HS-1-6.1	1.76	99	58	0.59	5.25	0.01955 (2.8)	0.089 (54)	0.033 (54)	124.8±3.5	92±29
HS-1-7.1	3.34	193	230	1.19	1.26	0.01984 (1.8)	0.134 (10)	0.0489 (10)	126.6±2.2	120.8±5.1
HS-1-8.1	3.80	220	143	0.65	1.96	0.01973 (1.9)	0.106 (20)	0.0389 (19)	125.9±2.3	119±12
HS-1-9.1	6.03	349	269	0.77	1.78	0.01976 (1.7)	0.122 (15)	0.0450 (15)	126.1±2.2	118.0±8.8
HS-1-10.1	3.81	221	176	0.80	0.76	0.01991 (1.7)	0.1384 (5.7)	0.0504 (5.4)	127.1±2.1	125.7±4.4
HS-1-11.1	15.8	907	379	0.42	0.05	0.02032 (1.5)	0.1415 (2.9)	0.0505(2.4)	129.7±1.9	129.5±3.8
HS-1-12.1	3.79	214	117	0.55	2.20	0.02015 (2.3)	0.108 (28)	0.039 (28)	128.6±3.0	112±20
HS-2-1.1	2.82	167	97	0.58	1.45	0.01938 (2.1)	0.138 (18)	0.0516 (17)	123.7±2.5	126±15
HS-2-2.1	10.3	600	296	0.49	0.82	0.01975 (1.5)	0.1240 (5.2)	0.0455 (4.9)	126.1±1.9	119.6±4.5
HS-2-3.1	4.78	294	193	0.66	1.39	0.01866 (1.6)	0.1328 (7.1)	0.0516 (6.9)	119.2±1.9	104.6±5.4
HS-2-4.1	2.04	116	88	0.76	3.54	0.01973 (2.0)	0.103 (23)	0.0378 (23)	126.0±2.5	114±11
HS-2-5.1	8.70	496	225	0.45	2.20	0.02000 (1.6)	0.108 (13)	0.0393 (13)	127.6±2.0	94±11
HS-2-6.1	1.48	84	53	0.63	0.00	0.02080 (2.3)	0.220 (14)	0.077 (14)	132.7±3.1	177±19
HS-2-7.1	2.47	142	80	0.56	4.91	0.01932 (2.3)	0.053 (64)	0.020 (64)	123.4±2.8	77±22
HS-2-8.1	1.87	100	93	0.93	8.82	0.01990 (4.0)			127.0±5.0	83±25
HS-2-9.1	1.77	104	98	0.94	6.36	0.01860 (3.5)	0.077 (82)	0.030 (82)	118.8±4.2	114±24
HS-2-10.1	9.42	547	503	0.92	0.76	0.01990 (1.5)	0.1328 (6.4)	0.0484 (6.2)	127.0±1.9	120.1±4
HS-2-11.1	5.22	296	146	0.49	3.28	0.01985 (1.8)	0.079 (27)	0.0290 (27)	126.7±2.3	81±16
HS-2-12.1	32.1	1918	1311	0.68	1.28	0.01926 (1.5)	0.1248 (4.7)	0.0470 (4.5)	123.0±1.8	118.8±3.6
HS-3-1.1	15.6	570	350	0.61	7.47	0.02947 (2.1)	0.099 (51)	0.024 (51)	187.2±3.9	125±31
HS-3-2.1	7.48	437	212	0.49	1.57	0.01964 (1.7)	0.141 (11)	0.0522 (11)	125.4±2.1	117±12
HS-3-3.1	4.05	233	129	0.55	1.81	0.01986 (1.8)	0.104 (12)	0.0381 (11)	126.8±2.2	103.2±7.9
HS-3-4.1	4.99	290	94	0.32	4.73	0.01914 (2.2)	0.109 (29)	0.041 (29)	122.2±2.6	109±36
HS-3-5.1	3.43	203	125	0.62	1.79	0.01930 (1.8)	0.125 (13)	0.0469 (13)	123.3±2.2	115.9±9.9
HS-3-6.1	11.9	693	287	0.41	0.55	0.01984 (1.5)	0.1382 (5.8)	0.0505 (5.6)	126.6±1.9	122.0±6.5
HS-3-7.1	1.82	106	79	0.75	5.83	0.01890 (3.7)			120.7±4.6	83±34
HS-3-8.1	2.58	151	106	0.70	3.15	0.01929 (2.2)	0.106 (23)	0.0399 (23)	123.1±2.8	106±13
HS-3-9.1	5.68	330	205	0.62	6.17	0.01881 (2.0)	0.105 (26)	0.040 (26)	120.2±2.4	86±17
HS-3-10.1	9.30	533	256	0.48	0.00	0.02032 (1.5)	0.1564 (3.0)	0.0558 (2.6)	129.7±1.9	136.0±3.6
HS-3-11.1	1.73	108	120	1.11	8.81	0.01708 (3.4)	0.106 (53)	0.045 (53)	109.1±3.8	108±19
HS-3-12.1	1.21	67	54	0.81	2.71	0.02048 (3.4)	0.154 (41)	0.054 (41)	130.7±4.5	133±29
HS-4-1.1	261	224	6	0.86	0.33	0.0195 (15)	0.129 (22)	0.0478 (70)	125±9	122.9±20
HS-4-2.1	222	167	5	0.75	0.38	0.0196 (9)	0.121 (31)	0.0447 (109)	125±5	115.6±28
HS-4-3.1	6498	1638	120	0.25	0.37	0.0196 (26)	0.057 (62)	0.0211 (223)	125±16	56.2±57
HS-4-4.1	844	376	18	0.45	1.17	0.0213 (15)	0.144 (24)	0.0489 (69)	136±9	136.2±21
HS-4-6.1	208	156	4	0.75	0.25	0.0193 (18)	0.142 (27)	0.0533 (82)	123±11	134.7±24
HS-4-7.1	1723	1412	35	0.82	0.48	0.0184 (25)	0.055 (60)	0.0218 (229)	118±15	54.8±55
HS-4-8.1	197	150	4	0.76	0.29	0.0191 (18)	0.110 (21)	0.0418 (66)	122±11	105.9±19
HS-4-9.1	3410	2396	67	0.70	0.64	0.0181 (15)	0.116 (19)	0.0465 (64)	116±9	111.5±17
HS-4-10.1	92	60	2	0.65	0.58	0.0190 (15)	0.105 (29)	0.0401 (102)	121±9	101.4±26
HS-4-11.1	169	94	4	0.56	0.47	0.0213 (20)	0.134 (23)	0.0457 (59)	136±12	127.6±20
HS-4-13.1	13319	4530	272	0.34	0.93	0.0206 (17)	0.126 (13)	0.0443 (26)	131±10	120.1±12
HS-4-14.1	366	328	8	0.90	0.13	0.0188 (33)	0.090 (57)	0.0348 (203)	120±21	87.7±54

a) Errors are 1σ; Pb* indicates the radiogenic portions; f^{206}(%) is percent of common Pb in whole Pb.

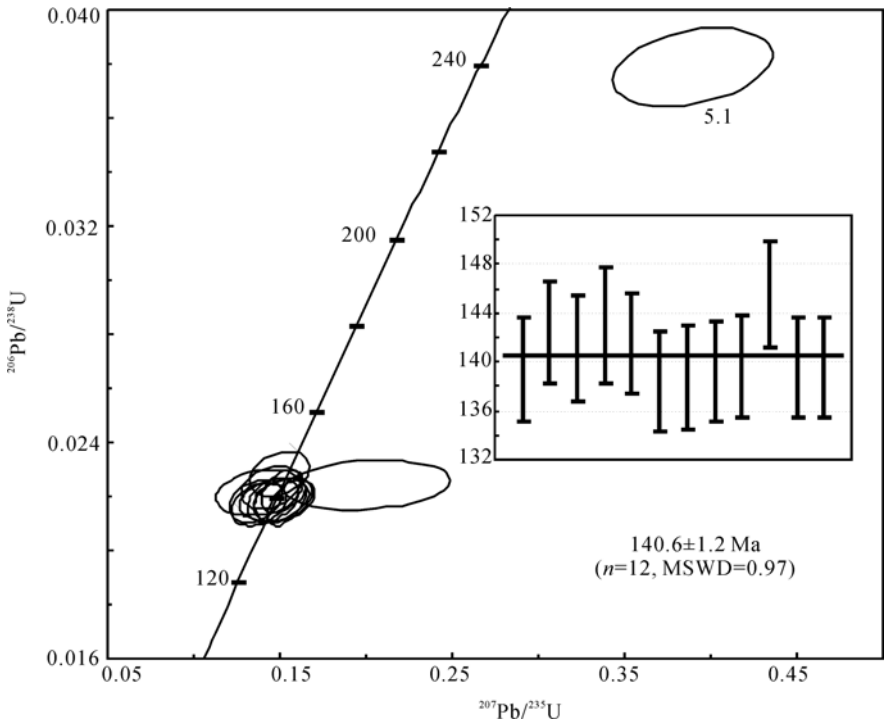

Figure 4 Concordia diagram showing SHRIMP analytical results for zircons from the Taiping granodiorite.

ple HS-2 are 119－133 Ma, with a weighted mean age of 125.7 ± 1.4 Ma (MSWD=1.30); the $^{206}Pb/^{238}U$ apparent ages of zircons from sample HS-3 are 119－133 Ma, with a weighted mean age of 125.1 ± 1.5 Ma (MSWD=1.80); $^{206}Pb/^{238}U$ apparent ages of zircons from sample HS-4 are 116－136 Ma, with a weighted mean age of 125.2 ± 5.5 Ma (MSWD=0.39). These four ages are consistent within error, indicating different stages or phases of the Huangshan intrusion were intruded in a short time. In $^{206}Pb/^{238}U$-$^{207}Pb/^{235}U$ concordia diagram, all analyses are located on or close by concordia (Figure 5).

4 Discussions and conclusions

4.1 Emplacement ages of the composite intrusion

In the early literature, the emplacement of the Taiping intrusion was ascribed to the Indo-Chinese event[48,49] without any isotopic age evidence. Zhao et al.[25−27] still claimed the Indo-Chinese event in their later papers. Zhou et al.[50] doubted an Indo-Chinese age of magmatism for the whole of Anhui Province, and obtained a biotite ^{40}Ar-^{39}Ar spectrum age of 137.1 Ma for granodiorite of the Taiping intrusion, which prior to this study is the only relatively precise age for it. The zircon SHRIMP U-Pb age of 140.6 ± 1.2 Ma for the granodiorite we report here is interpreted as the emplacement time of the Taiping intrusion.

As for the emplacement age of the Huangshan intrusion, Zhou et al.[50] obtained a biotite ^{40}Ar-^{39}Ar spectrum age of 125 Ma for the coarse- to medium-grained porphyritic granite. Using whole rock samples from different stages and phases of the Huangshan intrusion, Zhao et al.[25] obtained a Rb-Sr errochron of 124 Ma. In the 1∶200000 scale geological map of Jingde, the Huangshan intrusion was divided into two generations of granite (main generation) and porphyritic granite; whereas in the 1∶50000 scale geological maps of Taiping County and Tangkou, the Huangshan intrusion was divided into four units: the first is medium-grained monzogranite (Wenquan unit), the second is coarse-grained porphyritic granite (Yungusi unit), the third is medium-grained porphyritic granite (Shizifeng unit), and the fourth is fine-grained porphyritic granite (Gongyangshan unit). This was not supported by isotopic dating evidence, and in the field these units appear transitional into each other rather than having an intrusive relationship. Our analytical results indicate that the zircon U-Pb SHRIMP ages of different units or phases of the Huangshan intrusion are from 125 to 128 Ma, and consistent with each other within analytical errors. Therefore the “units” can be regarded as facies changes of the same intrusion.

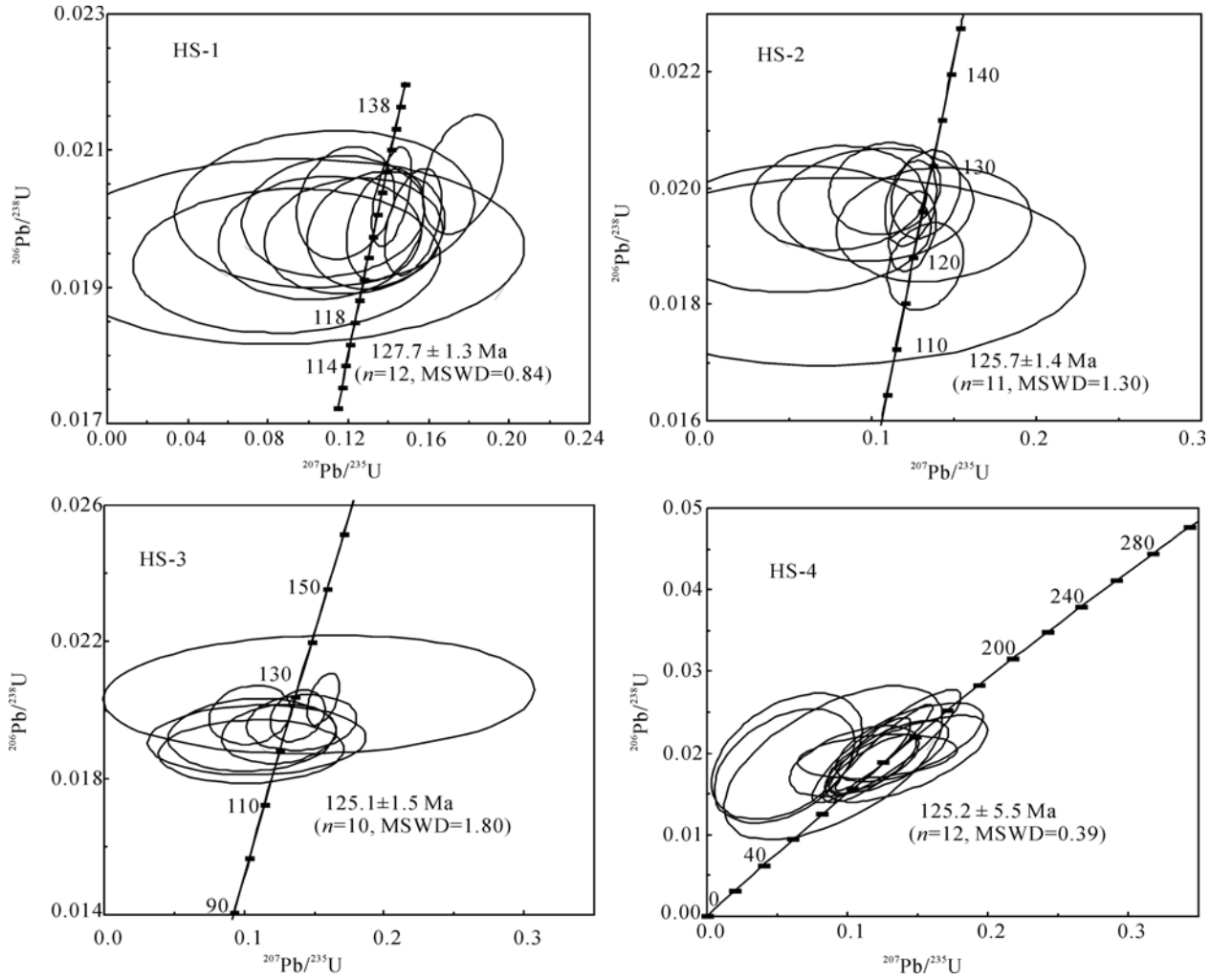

Figure 5 Concordia diagram showing SHRIMP analytical results for zircons from the Huangshan intrusive.

There is an interval of about 15 Ma from the emplacement of calc-alkaline Taiping intrusion to that of alkaline Huangshan intrusion. This suggests important changes happened in the tectonic setting of the southeastern Yangtze Craton and magma sources during this short time.

4.2 Temperature of the composite magma

Watson and Harrison[51] experimental obtained a function between Zr saturation and magma temperature:

$$T_{Zr}=12900/[2.95+0.85M+\ln(496000/Zr_{melt})],$$

$$M=(Na+K+2Ca)/(Al\times Si)\ (\text{unit: mol\%}),$$

where Zr_{melt} represents Zr content.

The Taiping intrusion and the Huangshan intrusion all have inherited zircon, indicating Zr saturation when the melts crystallized. The Zr saturation temperature of the Taiping intrusion sample is 768℃, and temperatures of the Huangshan intrusion samples are 811－764℃ (811, 802, 764 and 768℃ respectively, with an average of 786℃). The Zr saturation temperature of central unit of the Huangshan intrusion (sample HS-1) is 40℃ above the Taiping intrusion. Given the Huangshan intrusion comprises highly evolved magmatic differentiates and represents the transitional product from a magmatic system into a high-temperature hydrothermal system, its original magma should have been hotter. Therefore temperatures were raised after the crystallization of the Taiping intrusion, resulting in the formation of high temperature Huangshan A-type granitic magma, and a large amount of heat and material from asthenospheric mantle contributed to the magma formation.

4.3 Rock genesis

The Taiping-Huangshan composite intrusion was formed in a post-orogenic tectonic setting[24]. There are similar calc-alkaline to alkaline composite intrusions in the southeastern Yangtze Craton, such as Qingyang (calc-alkaline)-Jiuhuashan (alkaline) composite intrusion,

Leihu (calc-alkaline)-Guniujiang (alkaline) composite intrusion, Jiaocun (calc-alkaline)-Maotianshan (alkaline) composite intrusion etc. The mechanisms of magmatism in a post-orogenic setting include delamination[52,53], lithosphere convective removal[54], and slab break off[55]. All these mechanisms can result in upwelling of asthenospheric mantle, which in turn results in decompression melting of the upper asthenosphere or partial melting of subcontinental lithospheric mantle, and partial melting of lower crust caused by underplating of mantle derived magma. Mixing of these magmas from different sources can form many kinds of hybrid magma. Davies et al.[55] proposed that subcontinental lithospheric mantle would melt if the depth of delamination happened at less than 50 km, whereas decompression melting of asthenospheric mantle would happen if delamination occurred at a greater depth. In any mechanism, heat and material from the mantle have crucial influence on magmatism in a post-orogenic setting. In recent decades, large amounts of Sm-Nd and Rb-Sr whole rock isotopic data also indicate that mantle source material occupies a dominant role in the genesis of A-type granites[56−61].

Generally, A-type granites include alkaline granite with alkaline supersaturated and aluminous A-type granite[62−65]. The Huangshan intrusion is classified geochemically as aluminous A-type granite. For the genesis of aluminous A-type granites, King et al.[62] considered that it came from partial melting of felsic lower crust with normal H_2O contents. Poitrasson et al.[63,64] also proposed that the aluminous A-type granite came from partial melting of lower crust material, but considered that the source component was predominantly mafic; whereas Anderson et al.[65] considered that aluminous A-type granite came from partial melting of peraluminous sedimentary rocks in the lower crust. The basement of the Yangtze Craton where the Taiping-Huangshan composite intrusion is located includes high-grade metamorphic crystalline rocks and low-grade metamorphic folded rocks. Their $\varepsilon_{Nd}(t)$ values (corrected to the time of the Taiping-Huangshan intrusion) are usually below –20[44,66]. On the other hand, lithospheric mantle under ancient cratons is generally enriched[67,68], and research on the lithospheric mantle under the Yangtze Craton indicates a metasomatic enriched character[69−71]. The Sr, Nd isotopic composition of the Taiping intrusion can be simulated by a mixture of Yangtze Craton lower crust and depleted mantle then contaminated by upper crust (Figure 6). In contrast to the Taiping intrusion, the Huangshan intrusion has a lower initial $^{87}Sr/^{86}Sr$ ratio (about 0.707) and higher $\varepsilon_{Nd}(t)$ value (–4.45 to –4.87), similar to lithospheric mantle under the Yangtze Craton (Figure 6). Its relatively young depleted mantle Nd isotope model age (1.24−1.33 Ga) indicates that much depleted mantle material contributed to the source magma.

Until now, Mesozoic lithospheric thinning mechanisms proposed for eastern China are mainly delamination[1−4,6−8] and thermal erosion[9−14]. The former em-

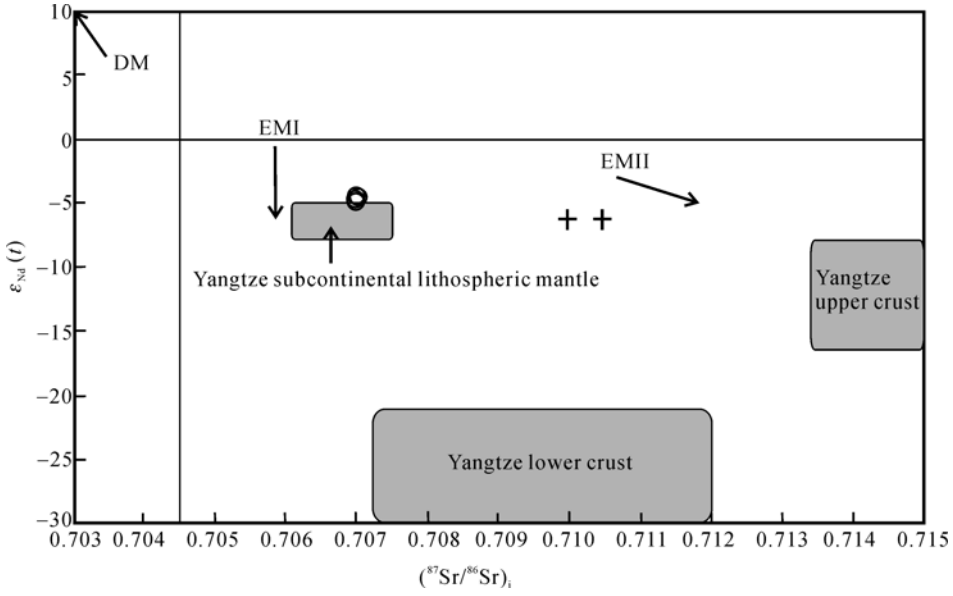

Figure 6 Diagram of $\varepsilon_{Nd}(t)$-$(^{87}Sr/^{86}Sr)_i$ Taiping-Huangshan intrusive.

phasizes dense lithospheric material "suddenly" sinking, whereas the latter emphasizes low density asthenosphere "gradually" upwelling. The Taiping and the Huangshan intrusions are intimately associated and constitute a composite intrusion, but there is an interval about 15 Ma between their emplacement, and the magma changed from calc-alkaline to alkaline, without transition. This probably indicates that the lithosphere was mainly thinned by mechanical delamination. It may be assumed that during the Indo-Chinese to early Yanshan stage, the region underwent far-field intra-continental orogenesis under the regional dynamic background of convergence of the North China Craton in the north and the South China Plate (the Cathaysian Block and South China Caledonian fold belt) in the south. This caused the lithosphere of the eastern Yangtze Craton to be thickened. During the post-orogenic stage, the thickened lithosphere started to delaminate and initiated asthenospheric mantle upwelling. Upwelling asthenospheric mantle triggered decompression melting and underplating in the crust-mantle interface, and resulted in partial melting of lower crustal rocks. The two types of magma mixed and ascended into the crust and were contaminated by upper crust to form the Taiping intrusion. Delamination triggered partial melting in the enriched subcontinental lithospheric mantle, with that magma mixing with magmas formed by decompression melting of upwelling asthenospheric mantle. This resulted in high temperature alkaline granitic magma, which was strongly differentiated (as well as contaminated) in the upper crust, finally forming the Huangshan granite.

The authors would like to thank professor Allen P Nutman for improving English of this paper and thank reviewers for their suggestion.

1 Deng J F, Mo X X, Zhao H L, et al. Lithosphere root/de-rooting and activation of the east China continent (in Chinese with English abstract). Geoscience, 1994, 8: 349－356

2 Deng J F, Su S G , Mo X X, et al. Deep processes of Mesozoic Yanshanian lithosphere thinning in North China (in Chinese with English abstract). Earth Sci Front, 2003, 10: 41－50

3 Gao S, Roberta L R, Richard W C, et al. Removal of lithospheric mantle in the North China Craton: Re-Os isotopic evidence for coupled crust-mantle growth (in Chinese with English abstract). Earth Sci Front, 2003, 10: 61－67

4 Gao S, Rudnick R L, Yuan H L, et al. Recycling lower continental crust in the North China Craton. Nature, 2004, 432: 892－897

5 Lu F X, Zheng J P, Shao J A, et al. Asthenospheric upwelling and lithospheric thinning in late Cretaceous-Cenozoic in eastern North China (in Chinese with English abstract). Earth Sci Front, 2006, 13: 87－92

6 Wu F Y, Sun D Y. The Mesozoic magmatism and lithospheric thinning in eastern China (in Chinese with English abstract). J Changchun Univ Sci Tech, 1999, 29: 313－318

7 Wu F Y, Ge W C, Sun D Y, et al. Discussions on the lithospheric thinning in eastern China (in Chinese with English abstract). Earth Sci Front, 2003, 10: 51－60

8 Xu W L, Wang Q H, Wang D Y, et al. Processes and mechanism of Mesozoic lithospheric thinning in eastern North China Craton: Evidence from Mesozoic igneous rocks and deep-seated xenoliths (in Chinese with English abstract). Earth Sci Front, 2004, 11: 309－317

9 Xu Y G. Roles of thermo mechanic and chemical erosion in continental lithospheric thinning (in Chinese with English abstract). Bull Mineral Petrol Geochem, 1999, 18: 1－5

10 Xu Y G. Lithospheric thinning beneath North China: A temporal and spatial perspective (in Chinese with English abstract). Geol J China Univ, 2004, 10: 325－331

11 Xu Y G, Huang X L, Ma J L, et al. Crust-mantle interaction during the tectono-thermal reactivation of the North China Craton: Constraints from SHRIMP zircon U-Pb chronology and geochemistry of Mesozoic plutons from western Shandong. Contrib Mineral Petrol, 2004, 147: 750－767

12 Zhang H F, Zhou X H, Fan W M, et al. Nature, composition, enrichment processes and its mechanism of the Mesozoic lithospheric mantle beneath the southeastern North China Craton (in Chinese with English abstract). Acta Petrol Sin, 2005, 12: 1271－1280

13 Zhang H F. Transformation of lithospheric mantle through peridotite-melt reaction: A case of Sina-Korean craton. Earth Planet Sci Lett, 2005, 237: 768－780

14 Zheng J P, Lu F X, Griffin W L, et al. Lithospheric thinning accompanying mantle lateral spreading, erosion and replacement beneath the eastern part of North China: Evidence from peridotites (in Chinese with English abstract). Earth Sci Front, 2006, 13: 77－85

15 Zhou X H. Major transformation of subcontinental lithosphere beneath eastern China in the Cenozoic-Mesozoic: Review and prospect (in Chinese with English abstract). Earth Sci Front, 2006, 13: 50－64

16 Ji S C, Wang Q, Xu Z Q. Break-up of the North China Craton through lithospheric thinning (in Chinese with English abstract). Acta Geol Sin, 2008, 82(2): 174－193

17 Xu X S, O'Reilly S Y, Griffin W L, et al. The nature of the Cenozoic lithosphere at Nushan, eastern China. In: Flower M, Chung S L, Lo C H, et al., eds. Mantle Dynamics and Plate Interactions in East Asia. Geodynamics Series, 27. Washington D C: American Geophysical Union, 2001. 167－196

18 Xu X S, O'Reilly S Y, Griffin W L, et al. Genesis of young lithospheric mantle in Southeastern China: An LAM-ICPMS trace element study. J Petrol, 2000, 41: 111－148

19 Whalen J B, Currie K L, Chappell B W. A-type granites: Geochemical characteristics, discrimination and petrogenesis. Contrib Mineral Petrol, 1987, 95: 407－419

20 Sylveter J P. Post-collisional alkaline granites. J Geol, 1989, 97: 261－280
21 Rogers J J W. Greenberg J E. Late-orogenic, post-orogenic, and anorogenic granites: Distinction by majorelement and trace-element chemistry and possible origins. J Geol, 1990, 98: 291－310
22 Eby G N. The A-type granitoids: A review of their occurrence and chemical characteristics and speculation on their petrogenesis. Lithos, 1990, 26: 115－134
23 Eby G N. Chemical subdivision of the A-type granitoids: Petrologic and tectonic implications. Geology, 1992, 20: 641－644
24 Xue H M, Wang Y G, Ma F, et al. The Huangshan A-type granites with tetrad REE: Constraints on Mesozoic lithospheric thinning of the southeastern Yangtze craton (in Chinese with English abstract)? Acta Geol Sin, 2009, 83: 247－259
25 Zhao L Z, Liu C S, Sun N. The petrological characteristics of the Taiping-Huangshan polygenetic composite batholith in southern Anhui (in Chinese with English abstract). J Nanjing Univy (Nat Sci), 1983, (2): 329－340
26 Zhao L Z, Liu C S. The composition and structural states of K-feldspars from Taiping-Huangshan polygenetic composite granitoid batholiths, Anhui (in Chinese with English abstract). J Mineral Petrol, 1987, 7: 39－50
27 Zhao L Z, Chen T H, Qian H D, et al. The composition and spectroscopic features of biotite from Huangshan-Taiping composite granitoid batholith (in Chinese with English abstract). Acta Mineral Sin, 1990, 10(2): 132－139
28 Huang J Q. Main Geotectonic Units of China (in Chinese). Geological Special of China Geological Survey, 1945. 20
29 Guo L Z, Si Y S, Ma R S. Geotectonic Framework and Crust Evolution of South China. Beijing: Geology Press, 1980. 109－116
30 Zhu X. Geodynamic setting of the Mesozoic-Cenozoic oil-gas basins in China. In: Zhu X, ed. Tectonics of Oil-gas Basins in China (in Chinese). Beijing: Petroleum Industry Press, 1980. 61－70
31 Xu J H, Sun S, Li J L. South China orogene other than craton (in Chinese). Sci China Ser B, 1987, 101: 1107－1115
32 Qiu Y X, Zhang Y C, Ma W P. Tectonics and geological evolution of Xuefeng intra continental orogene, South China (in Chinese with English abstract). Geol J China Univ, 1998, 4: 432－443
33 Zhu G, Liu G S. Basic characteristics and Mesozoic orogenic process of the Jingnan intracontinental orogenic belt in southern Anhui (in Chinese with English abstract). Geotect Metal, 2000, 24: 103－111
34 Pearce J A, Harris N B W, Tindle A G. Trace element discrimination diagram for the tectonic interpretation of granitic rocks. J Petrol, 1984, 25: 956－983
35 Bau M. Controls on the fractionation of isovalent trace elements in magmatic and aqueous systems: Evidence from Y/Ho, Zr/Hf, and lanthanide tetrad effect. Contrib Mineral Petrol, 1996, 123: 323－333
36 Bau M. The lanthanide tetrad effect in highly evolved felsic igneous rocks——A reply to the comment by Pan Y. Contrib Mineral Petrol, 1997, 128: 409－412
37 Pan Y. Controls on the fractionation of isovalent trace elements in magmatic and aqueous systems: Evidence from Y/Ho, Zr/Hf, and lanthanide tetrad effect——A discussion of the article by Bau M (1996). Contrib Mineral Petrol, 1997, 128: 405－408
38 Irber W, Förster H J, Hecht L, et al. Experimental, geochemical, mineralogical and O-isotope constraints on the late-magmatic history of the Fichtelgebirge granites (Germany). Geol Rundsch, 1997, 86(Suppl): 110－124
39 Nutman A P, Bridgwater D，Fryer B J. The iron-rich suite from the Amitsoq gneisses of southern West Greenland: Early Archaean plutonic rocks of mixed crustal and mantle origin. Contrib Mineral Petrol, 1984, 87: 24－34
40 Le Maitre R W. A Classification of Igneous Rocks and Glossary of Terms. Oxford: Blackwell, 1989
41 Boynton W V. Geochemistry of the rare earth elements: Meteorite studies. In: Henderson P, ed. Rare Earth Element Geochemistry. Amsterdam: Elsevier, 1984. 63－114
42 McDonough W F, Sun S S. The composition of the Earth. Chem Geol, 1995, 120: 223－253
43 Chen J F, Zhou T X, Li X M, et al. Sr and Nd isotopic constraints on source regions of the intermediate and acid intrusions from southern Anhui Province (in Chinese with English abstract). Geochimica, 1993, 22: 261－268
44 Jahn B M, Wu F Y, Lo C H, et al. Crust-mantle interaction induced by deep subduction of the continental crust: Geochemical and Sr-Nd isotopic evidence from post-collisional mafic-ultramafic intrusions of the northern Dabie complex, central China. Cheml Geol, 1999, 157: 119－146
45 Williams I S. U-Th-Pb geochronology by ion microprobe. In: Mickibben M A, Shanks III W C, Ridley W I, eds. Applications of Micro Analytical Techniques to Understanding Mineralizing Processes. Rev Econ Geol, 1998, 7: 1－35
46 Claoue-Long J C, Compston W, Roberts J, et al. Two Carboniferous ages: A comparison of SHRIMP zircon dating with conventional zircon ages and $^{40}Ar/^{39}Ar$ analysis. In: Berggren W A, Kent D V, Aubry M P, et al., eds. Geochronology, Time Scales and Global Stratigraphic Correlation. SEPM Special Publication, 1995. 5: 3－31
47 Ludwig K R. Users Manual for Isoplot/Ex (rev. 2.49): A Geochronologica Toolkit for Microsoft Excel. Berkeley Geochronology Center, Special Publication No. la, 2001. 1－55
48 Guiyang Institute of Geochemistry, Chinese Academy of Sciences. Geochemistry of the Granitoids in Southern China. Beijing: Science Press, 1979
49 Department of Geology, Nanjing University. Granitoids with Different Ages and Metallogenic Relation in Southern China. Beijing: Science Press, 1981
50 Zhou T X, Chen J F, Li X M, et al. Has the Indo-Sinian magmatism occurred in Anhui Province (in Chinese with English abstract)? Acta Petrol Sin, 1988, 3: 46－53
51 Watson E B, Harrison T M. Zircon saturation revisited: Temperature and composition effects in variety of crustal magma types. Earth Planet Sci Lett, 1983, 64: 295－304
52 Bird P. Continental delamination and the Colorado Plateau. J Geophys Res, 1979, 84: 7561－7571
53 Black R, Liégeois J P. Cratons, mobile belts, alkaline rocks and continental lithospheric mantle: The Pan-African testimony. J Geol Soc London, 1993, 150: 89－98

54 Houseman G A, McKenzie D P, Molnar P J. Convective instability of a thickened boundary layer and its relevance for the thermal evolution of continental convergent belts. J Geophys Res, 1981, 86: 6115－6132
55 Davies J H, von Blanckenburg F. Slab breakoff: A model of lithospheric detachment and its test in the magmatism and deformation of collisional orogens. Earth Planet Sci Lett, 1995, 129: 85－102
56 Turner S P, Foden J D, Morrison R S. Derivation of some A type magmas by fractionation of basaltic magma: An example from the Pathaway Ridge, South Australia. Lithos, 1992, 28: 151－179
57 Whalen J B, Jenner J A, Longstaffe F J, et al. Geochemical and isotopic (O, Nd, Pb and Sr) constraints on A-type granite petrogenesis based on the Topsails igneous suite, Newfoundland Appalachians. J Petrol, 1996, 37: 1463－1489
58 Jahn B M, Wu F Y, Chen B. Granitoids of the Central Asian Orogenic Belt and continental growth in the Phanerozoic. Trans R Soc Edinb Earth Sci, 2000, 91: 181－193
59 Jahn B M, Capdevila R, Liu D, et al. Sources of Phanerozoic granitoids in the transect Bayanhongor-Ulan Baator, Mongolia: Geochemical and Nd isotopic evidence, and implications of Phanerozoic crustal growth. J Asian Earth Sci, 2004, 23: 629－653
60 Bonin B. Do coeval mafic and felsic magmas in postcollisional to within-plate regimes necessarily imply two contrasting, mantle and crustal, sources? A review. Lithos, 2004, 78: 1－24
61 Katzir Y, Eyal M, Litvinovsky B A, et al. Petrogenesis of A-type granites and origin of vertical zoning in the Katharina pluton, Gebel Mussa (Mt. Moses) area, Sinai, Egypt. Lithos, 2007, 95: 208－228
62 King P L, White A J R, Chappell B W, et al. Characterization and origin of aluminous A-type granites from the Lachlan Fold Belt, Southeastern Australia. J Petrol, 1997, 38: 371－391
63 Poitrasson F, Pin C, Duthou J L, et al. Aluminous subsolvus anorogenic granite genesis in the light of Nd isotopic heterogeneity. Chem Geol, 1994, 112: 199－219
64 Poitrasson F, Duthou J L, Pin C. The relationship between petrology and Nd isotopes as evidences for contrasting anorogenic granite genesis: Example of the Corsican Province (SE France). J Petrol, 1995, 36: 1251－1274
65 Anderson J L, Thomas W M. Proterozoic anorogenic two-mica granites: Silver Plume and St. Vrain batholiths. Geology, 1985, 13: 177－180
66 Ames L, Zhou G, Xiong B. Geochronology and isotipic character of ultrahigh-pressure metamorphism with implications for collision of the Sino-Korean and Yangtze Cratons, central China. Tectonics, 1996, 15: 472－489
67 Tarney J, Weaver B L. Mineralogy, petrology and geochemistry of the Scourie dykes: Petrogenesis and crystallization processes in dykes intruded at depth. In: Park R G, Tarney J, eds. Evolution of the Lewisian and Comparable Precambrian High Grade Terrains. Geol Soc Spec Publ, 1987, 27: 217－233
68 Condie K C. Sources of Proterozoic mafic dyke swarms: Constraints from Th/Ta and La/Yb ratios. Precambrian Res, 1997, 81: 3－14
69 Chen J F, Yan J, Xie Z, et al. Nd and Sr isotopic compositions of igneous rocks from the Lower Yangtze region in Eastern China: Constraints on Sources. Phys Chem Earth, 2001, 26: 719－731
70 Yan J, Chen J F, Yu G, et al. Pb isotopic characteristics of Late Mesozoic mafic rocks from the lower Yangtze region: Evidence for enriched mantle (in Chinese with English abstract). Geol J China Univ, 2003, 9: 195－206
71 Yan J, Chen J F, Xie Z, et al. Geochemistry of Late Mesozoic basalts from Kedoushan in the Middle and Lower Yangtze regions: Constraints on characteristics and evolution of the lithospheric mantle (in Chinese with English abstract). Geochimica, 2005, 34(5): 455－469